Pesquisas em Geociências

http://seer.ufrgs.br/PesquisasemGeociencias

Electron microprobe chemical U-Th-Pb and La-ICP-MS U-Pb dating of multiple hydrothermal and metamorphic events recorded in minerals of the Lagoa Real uraniferous albitites (Brazil)

Alexandre de Oliveira Chaves, Michael Tubrett, Simone Cristina Pires Avelar, Francisco Javier Rios, Geraldo Norberto Chaves Sgarbi, José Marques Correia Neves, James Vieira Alves, Kazuo Fuzikawa, Evandro Carele de Matos, Sônia Pinto Prates

Pesquisas em Geociências, 36 (2): 181-201, set./dez., 2009.

Versão online disponível em:
http://seer.ufrgs.br/PesquisasemGeociencias/article/view/17865

Publicado por

Instituto de Geociências

Informações Adicionais

Email: pesquisas@ufrgs.br
Políticas: http://seer.ufrgs.br/PesquisasemGeociencias/about/editorialPolicies#openAccessPolicy
Submissão: http://seer.ufrgs.br/PesquisasemGeociencias/about/submissions#onlineSubmissions
Diretrizes: http://seer.ufrgs.br/PesquisasemGeociencias/about/submissions#authorGuidelines

Data de publicação - set./dez., 2009.
Instituto de Geociências, Universidade Federal do Rio Grande do Sul, Porto Alegre, RS, Brasil

Pesquisas em Geociências, 36 (2): 181-201, mai./ago. 2009 ISSN 1518-2398
Instituto de Geociências, Universidade Federal do Rio Grande do Sul, Porto Alegre, RS, Brasil E-ISSN 1807-9806

Electron microprobe chemical U-Th-Pb and La-ICP-MS U-Pb dating of multiple hydrothermal and metamorphic events recorded in minerals of the Lagoa Real uraniferous albitites (Brazil)

Alexandre de Oliveira CHAVES[1], Michael TUBRETT[2], Simone Cristina Pires AVELAR[3], Francisco Javier RIOS[3], Geraldo Norberto Chaves SGARBI[4], José Marques Correia NEVES[3], James Vieira ALVES[3], Kazuo FUZIKAWA[3], Evando Carele de MATOS[5] & Sônia Pinto PRATES[3]

1. Universidade Federal do Espírito Santo. Alto Universitário, CEP 29500-000, Alegre-ES, Brazil.
E-mail: alochaves@yahoo.com.br.
2. Micro Analysis Facility, Inco Innovation Centre, c/o Memorial University of Newfoundland. 230 Elizabeth Avenue, P.O. Box 4200 St. John's, NL, A1C 5S7, Canada.
3. Centro de Desenvolvimento da Tecnologia Nuclear. Campus Universitário, Av. Pres. Antonio Carlos, 6627, CEP 31270-901, Belo Horizonte-MG, Brazil.
4. Instituto de Geociências da Universidade Federal de Minas Gerais. Campus Universitário. Av. Pres. Antonio Carlos, 6627, CEP 31270-000, Belo Horizonte-MG, Brazil.
5. Indústrias Nucleares do Brasil. Fazenda Cachoeira s/n, CEP 46400-000, Caetité-BA, Brazil.

Recebido em 12/2008. Aceito para publicação em 11/2009.
Versão *online* publicada em 14/06/2010 (*www.pesquisasemgeociencias.ufrgs.br*)

Resumo - Os albititos uraníferos de Lagoa Real são rochas que passaram por várias modificações após a formação. A datação química U-Th-Pb por microssonda eletrônica e datação U-Pb por LA-ICP-MS dos minerais dos albititos revelaram cristalização e metamorfismo isoquímico do protólito (sienitos sódicos portadores de U) em cerca de 2,0-1,9 Ga durante as fases finais do evento orogênico Orosiriano, quando a primeira geração de uraninitas foi formada. Mobilizações múltiplas de urânio e chumbo promovidas por pelo menos cinco eventos hidrotermais (1,7 Ga, 1,5 Ga, 1,3 Ga, 1,1 Ga e 1,0 Ga) foram detectadas nos albititos. A provável formação de um segundo grupo de uraninitas e/ou o reajuste do relógio U-Pb das uraninitas mais antigas durante o evento orogênico Brasiliano (0,5 Ga) também ocorreram.
Palavras-chave: idades químicas U-Th-Pb, idades U-Pb por LA-ICP-MS, albititos uraníferos, metamorfismo, hidrotermalismo.

Abstract - Lagoa Real uraniferous albitites are rocks which went through multiple modifications after formation. Electron microprobe chemical U-Th-Pb and LA-ICP-MS U-Pb dating of minerals of albitites reveal protolith (U-bearing sodic syenites) crystallization and isochemical metamorphism at ca. 2.0-1.9 Ga during the final stages of the Orosirian orogenic event, when the first generation of uraninites was formed. Multiple uranium and lead mobilization promoted by at least five hydrothermal events (ca. 1.7 Ga, ca. 1.5 Ga, ca. 1.3 Ga, ca. 1.1 Ga, and ca. 1.0 Ga) was detected in the albitites. A probable formation of a second uraninite group and/or resetting of U-Pb clock of older uraninites during the Brasiliano orogenic event at ca. 0.5 Ga also took place.
Keywords: chemical U-Th-Pb and LA-ICP-MS U-Pb ages, uraniferous albitites, metamosphism, hydrothermalism.

---

1. Introdução

Currently, there is only one active uranium mine in Latin America, located in the region of Lagoa Real (Bahia, Brazil) which is found in the central area of São Francisco Craton (Fig. 1). The Lagoa Real Uraniferous Province and its surroundings have been object of geological and aerogeophysical surveys (Costa *et al*., 1985; CPRM, 1995; Garrido *et al*., 2002) and of various studies on the origin and control of uranium deposits, including those of Geisel Sobrinho (1981), Alves & Fuzikawa (1984), Oliveira *et al*. (1985), Turpin *et al*., (1988), Maruéjol (1989), Lobato & Fyfe (1990), Pimentel *et al*. (1994), Pascholati *et al*. (2003), and Cruz (2004). Some of these studies attribute the genesis of the mineralization to uranium and sodium-bearing hydrothermal fluids, which would have metasomatised the ca. 1.7 Ga anorogenic São Timóteo Granite (granite age by Turpin *et al*., 1988; Cordani *et al*., 1992, and Pimentel *et al*., 1994) and partially transformed it into uraniferous albitites.

New evidence presented here, supported by LA-ICP-MS U-Pb (Chaves *et al*., 2007) and electron microprobe chemical U-Th-Pb dating, point out to an orogenic setting older than 1.7 Ga, involving uraniferous mineralization of Lagoa Real and to multiple uranium and lead mobilization. Hence, one question arises: are the albitites Na-metasomatised anorogenic granitic rocks or are they isochemically metamorphosed sodic syenites of orogenic setting? Therefore, the aim of the present study is to understand when orogenic felsic magmatism and subsequent metamorphic and thermal events which mobilized uranium and formed uraninite took place, as well as the implications for regional geological evolution.

2.Geological setting

The Lagoa Real region is located in the central-southern part of São Francisco Craton (Fig. 1). The basement of this region is formed of Archean/Paleoproterozoic granulite, migmatite, and gneiss, which belong to the Paramirim and Gavião blocks (Inda & Barbosa, 1996). The Ibitira-Brumado volcanosedimentary unit is found in the area and comprises amphibolite, banded iron formation, gneiss, metachert, marble, and schist. This unit was interpreted as a early Paleoproterozoic greenstone belt (Mascarenhas, 1973). The Paleoprotozoic Lagoa Real Granite-Gneiss Complex covers an area larger than 2,000 km^2 of the Paramirim Block and includes granitoid bodies, gneiss, albitite and amphibolite. Maruéjol (1989) attributes the genesis of the uranium-bearing albitites to metamorphism and progressive deformation of the 1.7 Ga anorogenic São Timóteo Granite along shear zones, where an episyenitization process controlled by uranium and sodium bearing hydrothermal fluids took place. Another important geological unit in the region is the Espinhaço Supergroup, comprising sandstone, conglomerate, siltstone, shale, quartzite and schist overlying a sequence of ca.1.7 Ga rhyolite and rhyodacite. This supergroup is related to a basin developed during upper Paleoproterozoic rifting event. Tertiary covers and Quaternary alluvial sediments complete the geological scenario of this region (Fig. 1). According to Almeida (1977) and Cordani & Brito Neves (1982), the geological and tectonic context of the Lagoa Real region is part of the evolution of the São Francisco Craton and successive orogenic cycles: Jequié (Archean), Transamazonian or Orosirian (Paleoproterozoic), and Brasiliano (Late Neoproterozoic). During the Brasiliano Orogeny, Archean gneiss basement overthrusted metasedimentary rocks of the Espinhaço Supergroup and therefore N-S regional thrust faults are found in Paramirim Block (Caby & Arthaud, 1987).

Uranium mineralization at Lagoa Real is found as finely disseminated (micro to milimetric) uraninite associated with discontinuous tabular bodies of albitites located along shear zones (Geisel Sobrinho, 1981; Ribeiro *et al.,* 1984; Costa *et al*., 1985; Turpin *et al*., 1988; Lobato & Fyfe, 1990; Cordani *et al*., 1992). Most bodies trend N40E to N30W and dip 30° to 90° to the southwest or northwest, with the exception of the northernmost deposits, which dip to the east, and those situated in the central part of the region, which are almost vertical. Each body may vary up to 3 km in length, averaging 10 m in width (max. 30 m). Mineralization extends up to 850 m below the surface as shown by drill cores (Ribeiro *et al*., 1984). Bodies contain one or more mineralized levels, which may be interrupted at certain places. The contacts between mineralized levels with host gneissic rocks is transitional or, in some cases, abrupt. According to Costa *et al*. (1985), amphibolites often occur along tabular bodies of albitites with the same structural trends and are also deformed by shear zones.

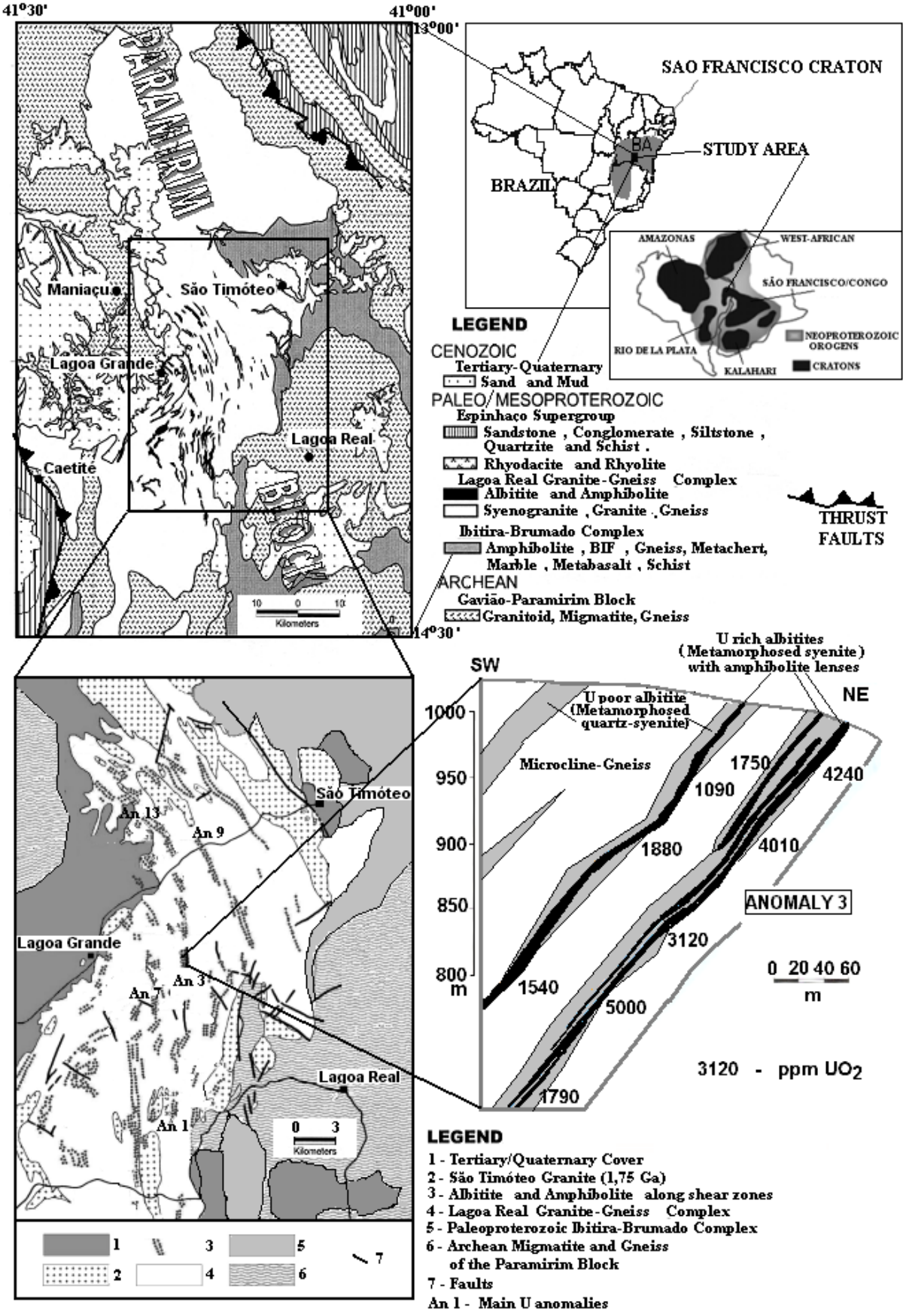

Figura 1. Geological setting of the Lagoa Real uraniferous albitites, Bahia (BA, Brazil). Modified from Pascholati *et al.* (2003) and Costa *et al.* (1985).

3. Methods

In order to understand the chronology of the geological events associated with the uraniferous mineralization of Lagoa Real, the following steps were undertaken: field work for geological survey and sample collecting from Cachoeira Mine pit (anomaly 13) and drill-core rocks from anomalies 1, 3, 7, and 9 of the Lagoa Real Uraniferous Province (Fig. 1). They are five lithostructurally similar coeval anomalies, with the same mineral paragenesis. Polished thin sections were prepared in the Laboratório de Preparação de Amostras of Centro de Desenvolvimento da Tecnologia Nuclear (CDTN) for petrographic and microanalytical/geochronologic studies. The petrography of several rock types from Lagoa Real region was carried out at Laboratório de Inclusões Fluidas e Metalogênese (LIF) at CDTN. A Leica DMR-XP microscope was used in the process.

For geochronological purposes, Pb/U isotope ratios in uraninite and zircon crystals of Lagoa Real albitites were determined by LA-ICP-MS technique (Laser Ablation Inductively Coupled Plasma Mass Spectrometry, reported by Sylvester, 2001), using zircon 91500 and uraninite TSA standards by Chaves *et al*. (2007). The coupled Laser Ablation (Cetac/GeolasPro- operating wavelength 193 nm, energy density 40J/cm^2 with spot size of 20 micrometers) and ICP-MS (Thermo/Element2 - sensitivi-ty 1x10^9 cps/ppm In, mass resolution 600, 8000, 20,000 FWHM, magnetic scan speed m/z 7 -> 240 to 7 < 150 ms, signal stability better than 2% over 1 hour) instruments used in this study are installed at the Memorial University of Newfoundland, St. John's, Canada.

Microanalyses of several mineral phases were carried out at the Physics Department of Universidade Federal de Minas Gerais (UFMG) with a Jeol-JXA-8900 RL WD/ED electron microprobe. Operating conditions were 15 kV (voltage) and 50 nA (current). Total counting time on a single spot was 600 s for U, Th and Pb and 40 s for all other elements. Ma line was chosen for U, Th, and Pb analysis. Despite the presence of a ThMβ line, the UMα-line was chosen rather than the UMβ line in order to gain a better counting rate. The spectral interference of ThMb on UMα was corrected online by measuring the background for U on the ThMβ line on the other side of the UMα line, symmetrically from the position of the ThMβ line.

LA-ICP-MS and electron microprobe microanalyses were performed on the same aforementioned polished thin sections. EPMA DATING software (Pommier *et al*., 2004) was used for chemical U-Th-Pb age calculation of each spot analyzed by electron microprobe. ISOPLOT software (Ludwig, 2003) was used to determine mineral ages for both LA-ICP-MS and electron microprobe techniques.

4. Results and discussion

4.1 Petrography, metamorphic reactions, and uraninite formation

Thirty representative polished thin sections of the Lagoa Real albitites were investigated. This investigation led to a better understanding of texture and mineral paragenesis as well as of metamorphic reactions that developed in the albitites, which are here understood as metamorphosed syenites (uraniferous) and quartz syenites (non uraniferous), according to the features described below.

The term albitite represents two distinct petrographic types in this work. Both are rich in albite, as the name indicates, and are closely related to ductile shear zones. The first one is a metamorphosed syenite without quartz but with associated uraniferous mineralization. The second one is a metamorphosed quartz-syenite. The second type differs from the first one due to its quartz, higher potassic feldspar content and lower volume of accessory minerals, and rare associated uraniferous mineralization. The mineralogy is nearly the same for both petrographic types.

The explanation for the quartz-free rocks being syenites and not hydrothermal albitites as previously suggested by Maruéjol (1989), Lobato & Fyfe (1990), and other authors was found during micropetrographic studies, which indicated strong anisotropy in the metamorphic foliation (heterogeneous deformation) generated during ductile shear development, as shown in figure 2. There are portions of the rock where the texture and the mineralogy of magmatic stage are preserved, including antiperthites. Other ones mix magmatic and metamorphic textures and many others have exclusively granoblastic texture. Therefore, the evolution of the transformation of the magmatic stage minerals during metamorphism up to their

complete recrystallization is evident. Besides the recrysta-llized minerals, new ones also resulted from metamorphic reactions. In preserved portions of the rock magmatic stage both quartz and features resembling silica dissolution were not found. Since quartz is absent in these portions, there is no reason to believe that quartz-rich São Timóteo Granite underwent sodic metasomatism to generate albitites. In portions that preserve the magmatic stage, albite (50% to 70% of rock volume), iron-rich augite (20% to 40%) and some microcline (up to 15%) are found as essential members and this composition classifies the rock as syenite. Accessory minerals of magmatic portions are dark brown uraniferous titanite [titanite crystals with high uranium concentra-tions have been reported by Gregory *et al*. (2005) and Pimentel *et al*. (1994), and can be understood as the replacement of Ti^{4+} for U^{4+} and, which have similar ionic radius], allanite-(Ce), magnetite, fluor-apatite, zircon, fluorite, and apophyllite. Magmatic calcite is sometimes present, which can be found inside undeformed augite crystals.

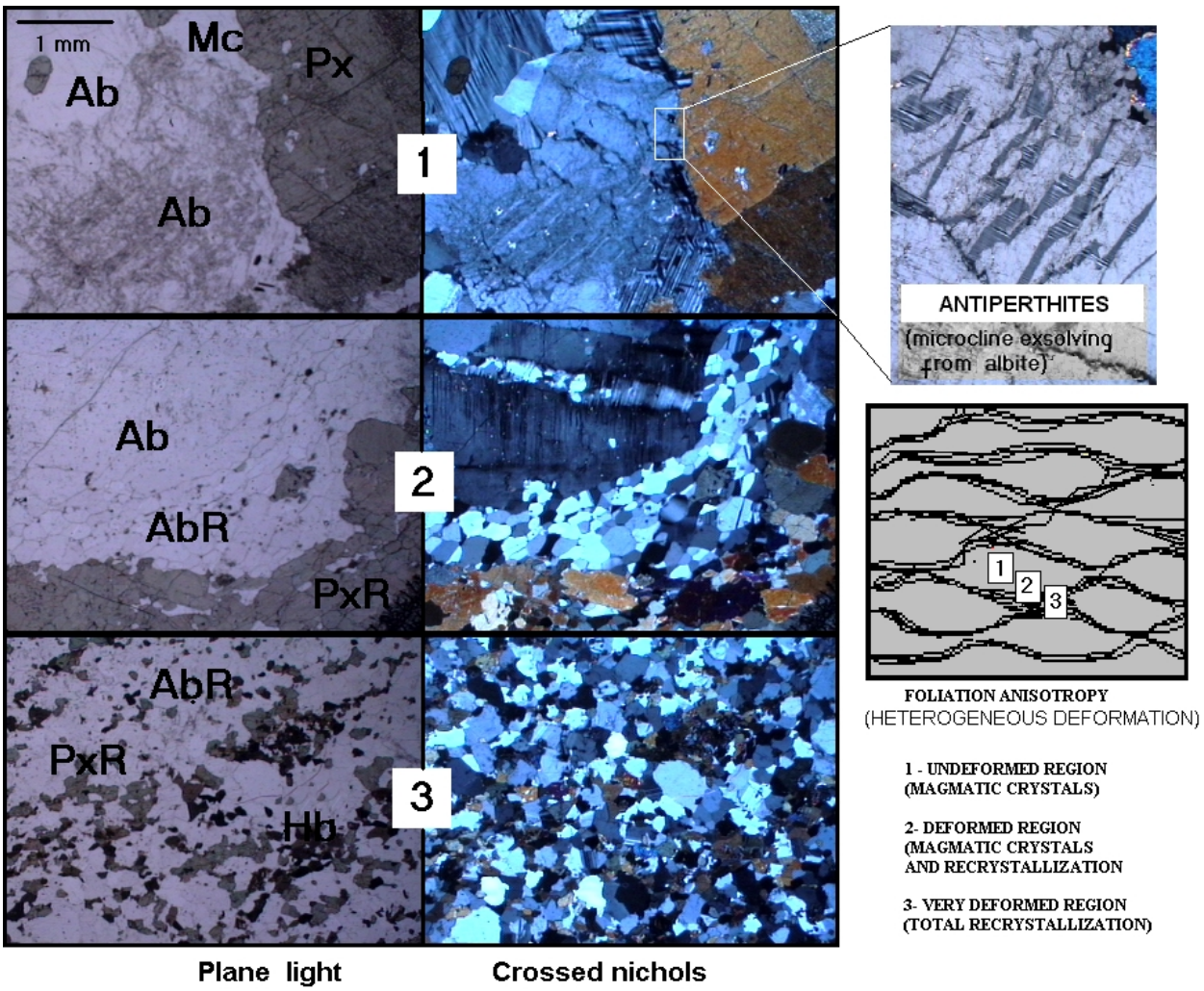

Figura 2. Anisotropy of metamorphic foliation in metamorphosed syenites. Pictures numbered 1 show the magmatic stage found in region 1 of the scheme on the right side of the figure. They include antiperthites with microcline exsolved from albite. Pictures numbered 2 show the initial stages of the metamorphic recrystallization and would be from region 2 of the scheme. The recrystallization of a large albite crystal, associated with the recrystallization of iron-rich augite can be noted. Pictures numbered 3 show the final stages of the metamorphic recrystallization, in which the well developed granoblastic texture can be observed and would be from region 3 of the scheme (largest deformation). Metamorphic hastingsite appears in region 3 (Ab – Magmatic albite, Px – Magmatic augite, Mc – Magmatic microcline, AbR – Albite recrystallized during metamorphism, PxR – Augite recrystallized during metamorphism, Hb – hastingsite, a hornblende).

In the first metamorphic stage, under high-grade amphibolite facies, not only hastingsite, but also andradite (Ca and Fe^{3+} garnet) resulting from iron-rich augite transformation were formed. Andradite became part of the metamorphosed syenite, rock formed through recrystallization of iron-rich augite, albite, microcline (± calcite), and accessory minerals. During recrystallization, iron-rich augite became aegirine-augite (more sodic) and albite became oligoclase (slightly more calcic). The association between oligoclase and andradite reveals high pressure metamorphism common to ductile shear zones (Yardley, 1989). Magnetite was replaced by hematite. Therefore, the mineralogical transformations reveal the rising of Fe^{3+} during metamorphism.

Uraninite, whose uranium derives essentially from uraniferous magmatic titanite (Fig. 3), was also formed. It was precisely from the transformations imposed on U-rich titanite, not only during metamorphism related to shear processes but also during hydrothermal events, that uranium became available in both reduced (tetravalent uranium) and more mobile oxidized forms (as uranyl ions - $UO_2^{+2,}$ in which uranium is hexavalent) to take part in chemical reactions which led to the formation of uraninite.

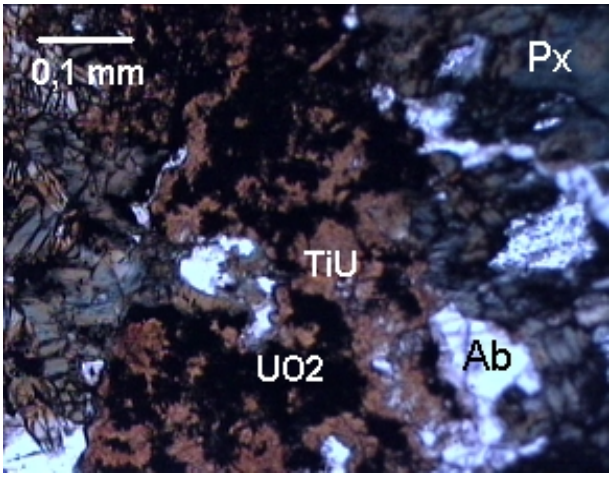

Figura 3. Uraniferous magmatic dark brown titanite (TiU) with uraninite (UO_2). Ab = albite. Px = pyroxene.

A chemical mechanism for the precipitation of uraninite, which would have a Redox (oxi-reduction) control in some steps, was suggested by Chaves *et al*. (2007):

STEP 1: The U^{4+} ions released from uraniferous titanite during either shear or hydrothermal events combined with OH^- ions released from the partial hydrolysis of albite, forming uraninite in a non-Redox process.

$$U^{4+} + 4OH^- \rightarrow UO_2 + 2H_2O \text{ [or } U(OH)_4\text{]} \text{ (step 1)}$$

STEP 2: In metamorphosed syenites without calcite, uraninite interacted completely or partially with the free oxygen circulating through the aqueous fluids during shear process. U^{4+} oxidized and became aqueous uranyl hydroxide complexes (with U^{6+}), which are stable under temperature and pressure conditions of the shear process (Finch & Murakami, 1999). In metamorphosed syenites with calcite, calcium carbonate was hydrolyzed and formed uranyl tricarbonate complex, which is very stable in the alkaline aqueous environment generated at this stage. Kojima *et al*. (1994) show that relative abundances of the uranyl tricarbonate complex in solution increase with increasing temperature, under relatively oxidizing and slightly alkaline conditions.

$$2UO_2 + 2H_2O + O_2 \rightarrow 2[UO_2(OH)_2]^0$$
(step 2 without calcite - Redox)

$$2UO_2 + 2H_2O + O_2 + 6CaCO_3 \rightarrow 2[UO_2(CO_3)_3]^{4-} + 4OH^- + 6Ca^{2+}$$
(step 2 with calcite - Redox)

The aqueous alkaline environment certainly facilitated the dissolution of silicates of the rock (silica solubility increases with increasing pH - Langmuir, 1997), and eventually uranyl hydroxisilicate complexes were formed which also helped in the mobilization of uranium.

$$2\ UO_2^{2+} + 2OH^- + SiO_4^{4-} \rightarrow [(UO_2)_2SiO_4(OH)_2]^{2-}$$

Orange-yellowish channels with chemical composition similar to iron-rich "uranophane" were found in albitites and probably represent the precipitation of uranyl hydroxisilicate anionic complexes in the presence of calcium and iron cations (Fig. 4). These channels are also rich in radiogenic lead (Tab. 1). It is important to point out that Fe and (radiogenic) Pb-rich "uranophane" has not been described in previous renowned papers (e.g. Finch & Murakami, 1999), and could be a new uranyl mineral species.

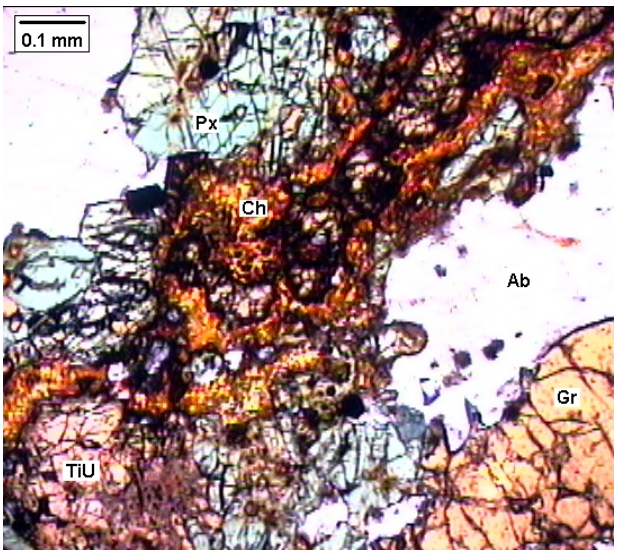

Figura 4. Channels with chemical composition similar to uranophane, but rich in radiogenic lead and iron. Ch - channel, Px - augite, Gr - andradite, Ab - albite/oligoclase, TiU - uraniferous titanite.

STEP 3: Although uranium became extremely mobile either as uranyl tricarbonate or uranyl hydroxisilicate, Fe^{2+} of magmatic augite led to reduction of U^{6+} to U^{4+} and to the precipitation of uraninite. The precipitated uraninite was retained inside recrystallized augite and calcite as well as inside andradite formed at that moment. In thin sections, we can clearly notice channels or surfaces containing uraninite which precipitated when the fluid containing U^{6+} passed through augite and reacted with Fe^{2+} (Fig. 5). Uraninite can also be seen in calcite recrystallized from a fluid containing uranyl tricarbonate which passed through augite and reacted with Fe^{+2} (Fig. 6). In metamorphosed syenites without calcite, uraninite precipitation as referred to in step 3 was restricted to the reaction in solution of uranyl ions with Fe^{2+} from iron-rich augite crystals. Uraninite-bearing andradite and the same uraninite-bearing channels or surfaces in recrystallized augite are seen in these metamorphosed syenites.

$$3Ca^{2+}+[UO_2(CO_3)_3]^{4-}+2Fe^{2+} \rightarrow UO_2+2Fe^{3+}+3CaCO_3$$
(step 3 with calcite - Redox)

$$UO_2{}^{2+} + 2Fe^{2+} \rightarrow UO_2 + 2Fe^{3+}$$
(step 3 without calcite - Redox)

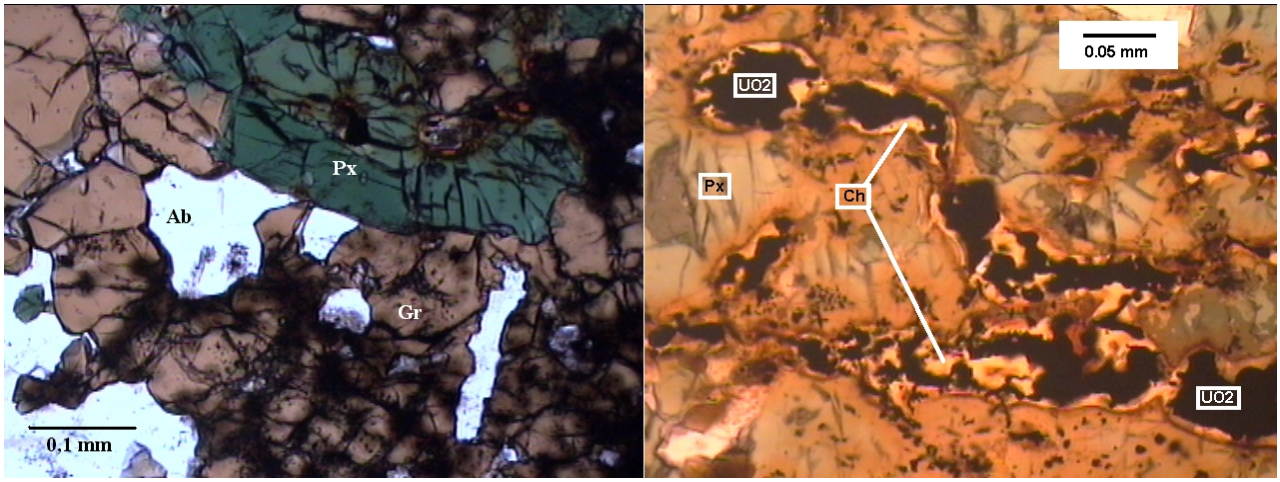

Figura 5. Uraninite (in black, metamictic) inside andradite (Gr -on the left). On the right side, another picture showing channels that contain uraninite (in black) inside recrystallized augite (Px). Uraninite (UO_2) precipitated in the channels (Ch -composition similar to those of figure 4) from a solution containing U^{6+} that reacted through a Redox process with the Fe^{2+} of augite crystals when it passed through them. Ab = albite/oligoclase.

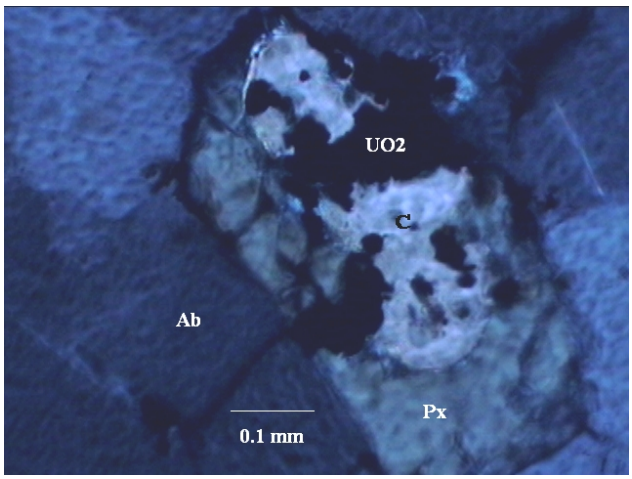

Figura 6. Recrystallized calcite (C) with uraninite (UO_2) inside augite (Px). Ab = albite/oligoclase.

Lobato & Fyfe (1990) previously suggested that uraninite precipitation in Lagoa Real was controlled by the reduction of an uraniferous fluid phase, via progressive oxidation of mafic minerals.

Epidote and biotite appeared during a second metamorphism stage. They partially replaced the minerals formed during the initial metamorphism. This paragenesis indicates re-equilibrium established under new temperature and pressure conditions, less intense than the ones that formed garnet during the initial metamorphism. It is interesting to notice that uraninite crystals are found inside epidote and biotite and also probably have precipitation related to Redox processes (both Fe^{2+} and Fe^{3+} appear in biotite while in epidote only Fe^{3+}). Uraninite precipitation inside these minerals, eventually with involvement of calcite, should have occurred under these new metamorphic conditions between greenschist and amphibolite facies.

Cenozoic microfracturing affected Lagoa Real albitites, crosscutting their metamorphic foliation. Fractures were filled by ordinary uranophane, autunite, and calcite.

4.2 Geochronology

For geochronological purposes, zircon, uraninite, allanite-(Ce), epidote, uraniferous titanite, iron and lead-rich "uranophane", ordinary uranophane, and autunite were investigated by electron microprobe. Representative average chemical analyses of these minerals from anomalies 1, 3, 7, 9 and 13 are shown in table 1. Spot ages in such minerals and mineral average ages are presented in table 2.

Pb/U isotopic ratios obtained by LA-ICP-MS (Chaves *et al.*, 2007), which has been shown to be an efficient technique for geochronological studies (Pickhardt *et al.*, 2005), allowed to determine ages of zircon and uraninite crystals of Lagoa Real albitites. ^{204}Pb was not found in both minerals by using LA-ICP-MS and therefore lead can be understood as radiogenic. This fact makes age data obtained by electron microprobe reliable.

$^{206}Pb/^{238}U$ and $^{207}Pb/^{235}U$ ratios of rim and core areas of three zircon crystals of three different radioactive anomalies (3, 7, and 13) produced the U-Pb discordia presented in figure 7, which also shows the values of the Pb/U ratios of each zircon. An age of 1904 ± 44 Ma, corresponding to the upper intercept and an age of 483 ± 100 Ma, corresponding to the lower intercept have been found.

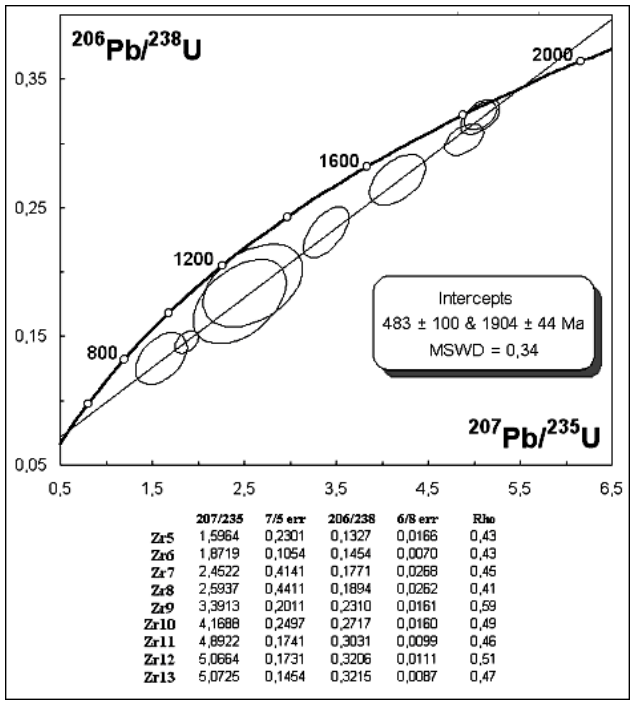

	207/235	7/5 err	206/238	6/8 err	Rho
Zr5	1,5964	0,2301	0,1327	0,0166	0,43
Zr6	1,8719	0,1054	0,1454	0,0070	0,43
Zr7	2,4522	0,4141	0,1771	0,0268	0,45
Zr8	2,5937	0,4411	0,1894	0,0262	0,41
Zr9	3,3913	0,2011	0,2310	0,0161	0,59
Zr10	4,1688	0,2497	0,2717	0,0160	0,49
Zr11	4,8922	0,1741	0,3031	0,0099	0,46
Zr12	5,0664	0,1731	0,3206	0,0111	0,51
Zr13	5,0725	0,1454	0,3215	0,0087	0,47

Figura 7. Zircon U-Pb discordia of uraniferous albitites (metamorphosed syenites). Error ellipses are 2s. Data sheet is also shown.

Taking into account that uraninite was formed during metamorphic events, its Pb/U isotopic ratio was also determined as uraninite serve as temporal indicators of these events. Andradite-related uraninite (first metamorphic event) and epidote-related uraninite (second metamorphic event) were chosen. Two different uraninite groups could be identified in terms of their isotopic ratios, one with $^{207}Pb/^{235}U$ around

0.7 for andradite-related uraninite and another with $^{207}Pb/^{235}U$ around 0.3 for epidote-related uraninite. The U-Pb discordia of these two groups of uraninite anchored to 0 Ma are given in figure 8, where values of Pb/U ratios of each crystal are also shown. Although there are not many data points along the discordia line, the first uraninite group shows a U-Pb system starting from a 1868 ± 69 Ma metamorphic episode (Fig. 8A). Despite the large error, the age of 605 ± 170 Ma (Fig. 8B) for uraninite crystals of the second group reveals another metamorphic event. Both metamorphic events seem also to be recorded by upper (ca. 1900 Ma) and lower (ca. 500 Ma) intercepts of the zircon U-Pb discordia (Fig. 7).

Table 1. Representative electron microprobe chemical analyses of U-(Th)-Pb-bearing minerals of the Lagoa Real albitites (values are in weight %. Total iron as FeO_T).

Mineral	Zircon	Allanite-(Ce)	Epidote	Uranif. Titanite	Fe and (radiog) Pb-rich "Uranophane"	Uraninite	Ordinary Uranophane	Autunite
SiO_2	33.41	34.23	34.84	27.87	16.37	1.42	20.51	0.00
TiO_2	0.00	0.00	0.00	31.51	0.00	0.00	0.00	0.00
Al_2O_3	0.00	13.23	18.41	1.38	0.00	0.00	1.11	0.00
FeO_T	0.26	14.37	18.76	2..29	7.36	0.00	0.00	0.00
MgO	0.00	0.50	0.30	0.00	0.00	0.00	0.00	0.05
CaO	0.04	13.33	22.45	27.83	3.17	5.61	7.18	6.35
P_2O_5	0.00	0.00	0.00	0.00	0.00	0.00	0.00	10.05
V_2O_3	0.00	0.00	0.00	2.06	0.00	0.00	0.00	0.00
Nb_2O_3	0.00	0.00	0.00	1.70	0.00	0.00	0.00	0.00
La_2O_3	0.00	5.39	0.00	0.00	0.00	0.00	0.00	0.00
Ce_2O_3	0.00	8.34	0.00	0.00	0.00	0.00	0.00	0.00
Nd_2O_3	0.00	4.12	0.00	0.00	0.00	0.00	0.00	0.00
UO_2	0.06	0.01	0.10	2.79	49.69	82.54	52.56	63.03
ThO_2	0.02	0.82	0.00	0.01	0.00	0.27	0.00	0.00
PbO	0.04	0.55	0.45	0.70	9.94	5.47	0.19	0.24
ZrO_2	64.34	0.00	0.00	0.00	0.00	0.00	0.00	0.00
HfO_2	1.01	0.00	0.00	0.00	0.00	0.00	0.00	0.00
H_2O	0.00	3.00	3.00	0.00	13.00	0.00	18.00	20.00
F	0.00	0.46	0.00	0.65	0.00	0.00	0.00	0.00
Total	99.18	98.35	98.31	98.79	99.53	95.31	99.55	99.72
Oxygens	16	13	13	20	20	2	20	20
		Si 3.197						
		Al 1.455		Si 3.947				
		Fe 1.122	Si 2.865	Al 0.230				
	Si 4.098	Mg 0.070	Al(IV) 0.135	Ti 3.357	Si 2.963		Si 3.057	
I	Zr 3.848	Ca 1.334	Al(VI) 1.648	U 0.090	Fe 1.114	Si 0.060	Al(VI) 0.20	P 1.380
O	Hf 0.040	Th 0.017	Fe3 1.160	V 0.230	U 2.000	U 0.780	Ca 1.146	U 2.280
N	Fe_2 0.027	Ce 0.285	Mg 0.037	Nb 0.11	Ca 0.615	Ca 0.255	U 1.740	Ca 1.107
S	Ca 0.005	La 0.185	Ca 1.978	Th 0.000	Pb 0.480	Pb 0.060	Pb 0.010	Pb 0.010
		Nd 0.137	U 0.000	Ca 4.223	OH 15.712		OH 17.909	OH 21.7
		U 0.000	Pb 0.010	Pb 0.030				
		Pb 0.014	OH 1.600	Fe2 0.27				
		OH 1.870		F 0.090				
		F 0.035						

Table 2. Electron microprobe U-Th-Pb chemical ages of some minerals of the Lagoa Real albitites by using EPMA Dating software (Pommier *et al*. 2004). (MPb = lead atomic mass). Weighted average ages calculated by using ISOPLOT software (Ludwig 2003).

Age (Ma)	Error Age (Ma)	U (ppm)	Error U (%)	Error U (ppm)	Th (ppm)	Error Th (%)	Error Th (ppm)	Pb (ppm)	Error Pb (%)	Error Pb (ppm)	MPb
ZIRCON											
975	620	722	8.31	60	99	60.61	60	113	53.10	60	206.118
1114	1385	282	21.28	60	133	45.11	60	56	100.00	56	206.280
1440	1987	188	31.91	60	58	100.00	58	48	100.00	48	206.212
1039	1311	229	26.20	60	0	100.00	0	37	100.00	37	206.045
598	654	643	9.33	60	0	100.00	0	57	100.00	57	206.032
773	690	643	9.33	60	0	100.00	0	75	80.00	60	206.037
Mean = 847 ± 680 Ma [80%] 95% conf.; Wtd by data-pt errs only. MSWD = 0.069. probability = 0.997											
URANIFEROUS TITANITE											
2191	241	1921	3.12	60	0	100.00	0	761	7.88	60	206.097
2028	202	2282	2.63	60	0	100.00	0	817	7.35	60	206.087
2088	86	25040	01/02/00	501	90	100.00	90	9320	2.00	186	206.093
2006	83	26170	2.00	523	110	100.00	110	9250	2.00	185	206.088
2130	92	17060	2.00	341	0	100.00	0	6510	2.30	150	206.093
1977	236	1956	3.07	60	0	100.00	0	677	8.86	60	206.085
1997	83	13285	2.00	266	70	85.32	60	4668	2.00	93	206.088
Mean = 2052 ± 80 Ma [3.9%] 95% conf.; Wtd by data-pt errs only. MSWD = 0.35. probability = 0.91											
1732	69	19990	2.00	400	0	100.00	0	5865	2.00	117	206.072
1693	73	9171	2.00	183	0	100.00	0	2617	2.29	60	206.070
1664	115	4352	2.00	87	0	100.00	0	1216	4.94	60	206.069
1656	98	5515	2.00	110	0	100.00	0	1531	3.92	60	206.068
1726	78	8180	2.00	164	0	100.00	0	2390	2.51	60	206.072
1727	69	22370	2.00	447	0	100.00	0	6540	2.00	131	206.072
1666	67	21230	2.00	425	0	100.00	0	5940	2.00	119	206.069
Mean = 1701 ± 57 Ma [3.4%] 95% conf.; Wtd by data-pt errs only. MSWD = 0.17. probability = 0.98											
1422	92	5815	2.00	116	9	100.00	9	1346	4.46	60	206.059
1481	67	9673	2.00	193	0	100.00	0	2348	2.56	60	206.061
1464	59	40330	2.00	807	0	100.00	0	9660	2.00	193	206.060
1558	62	19867	2.00	397	0	100.00	0	5123	2.00	102	206.064
1461	153	3154	2.00	63	114	52.51	60	761	7.88	60	206.079
Mean = 1488 ± 64 Ma [4.3%] 95% conf.; Wtd by data-pt errs only. MSWD = 0.49. probability = 0.74											
1291	161	2934	2.05	60	97	62.05	60	612	9.80	60	206.071
1330	72	8281	2.00	166	0	100.00	0	1772	3.39	60	206.055
1278	195	2317	2.59	60	0	100.00	0	473	12.68	60	206.053
1246	100	5048	2.00	101	0	100.00	0	1002	5.99	60	206.052
1277	66	9365	2.00	187	0	100.00	0	1912	3.14	60	206.053
1291	139	3462	2.00	69	141	42.66	60	724	8.29	60	206.075
1285	152	2978	2.01	60	0	100.00	0	612	9.80	60	206.053
1348	93	5594	2.00	112	0	100.00	0	1216	4.94	60	206.055
Mean = 1298 ± 69 Ma [5.3%] 95% conf.; Wtd by data-pt errs only. MSWD = 0.13. probability = 0.997											

Table 2. Cont.

Age (Ma)	Error Age (Ma)	U (ppm)	Error U (%)	Error U (ppm)	Th (ppm)	Error Th (%)	Error Th (ppm)	Pb (ppm)	Error Pb (%)	Error Pb (ppm)	MPb
1139	174	2590	2.32	60	0	100.00	0	464	12.93	60	206.048
1075	163	2810	2.13	60	35	100.00	35	473	12.68	60	206.053
1135	122	3850	2.00	77	0	100.00	0	687	8.74	60	206.048
1101	91	5779	2.00	116	123	48.76	60	1002	5.99	60	206.058
1108	59	10760	2.00	215	50	100.00	50	1870	3.21	60	206.049
1101	102	4793	2.00	96	0	100.00	0	826	7.26	60	206.047
Mean = 1108 ± 78 Ma [7.0%] 95% conf.; Wtd by data-pt errs only. MSWD = 0.027. probability = 1.000											
954	38	33160	2.00	663	10	100.00	10	4870	2.00	97	206.042
1034	52	12260	2.00	245	0	100.00	0	1970	3.05	60	206.044
1028	277	1647	3.64	60	132	45.51	60	269	22.29	60	206.088
1047	106	4555	2.00	91	0	100.00	0	742	8.08	60	206.045
933	58	9911	2.00	198	0	100.00	0	1420	4.23	60	206.041
1011	111	4317	2.00	86	18	100.00	18	677	8.86	60	206.046
Mean = 978 ± 50 Ma [5.1%] 95% conf.; Wtd by data-pt errs only. MSWD = 0.55. probability = 0.74											
Fe and (radiogenic) Pb-RICH "URANOPHANE"											
1707	68	396177	2.00	7924	589	10.19	60	114163	2.00	2283	206.072
1721	69	463732	2.00	9275	0	100.00	0	134978	2.00	2700	206.071
1714	69	418149	2.00	8363	0	100.00	0	121085	2.00	2422	206.071
1682	67	295003	2.00	5900	132	45.51	60	83474	2.00	1669	206.070
1754	70	78709	2.00	1574	2198	2.73	60	23627	2.00	473	206.087
Mean = 1715 ± 60 Ma [3.5%] 95% conf.; Wtd by data-pt errs only. MSWD = 0.14. probability = 0.97											
1491	60	430298	2.00	8606	0	100.00	0	105328	2.00	2107	206.061
1509	60	352858	2.00	7057	229	26.25	60	87603	2.00	1752	206.062
1485	59	294034	2.00	5881	0	100.00	0	71642	2.00	1433	206.061
1505	60	435628	2.00	8713	440	13.65	60	107843	2.00	2157	206.062
1468	59	415841	2.00	8317	0	100.00	0	99881	2.00	1998	206060
Mean = 1491 ± 52 Ma [3.5%] 95% conf.; Wtd by data-pt errs only. MSWD = 0.077. probability = 0.99											
1305	52	475432	2.00	9509	0	100.00	0	99509	2.00	1990	206.054
1275	51	412907	2.00	8258	598	10.04	60	84207	2.00	1684	206054
1298	52	488832	2.00	9777	105	56.88	60	101709	2.00	2034	206.054
1331	53	420096	2.00	8402	0	100.00	0	90007	2.00	1800	206.055
1291	52	437972	2.00	8759	0	100.00	0	90536	2.00	1811	206.053
1312	52	437795	2.00	8756	0	100.00	0	92225	2.00	1844	206.054
1313	53	474400	2.00	9488	0	100.00	0	100000	2.00	2000	206.054
1354	54	324900	2.00	6498	0	100.00	0	71000	2.00	1420	206.056
Mean = 1309 ± 36 Ma [2.8%] 95% conf.; Wtd by data-pt errs only. MSWD = 0.21. probability = 0.98											

Table 2. Cont.

Age (Ma)	Error Age (Ma)	U (ppm)	Error U (%)	Error U (ppm)	Th (ppm)	Error Th (%)	Error Th (ppm)	Pb (ppm)	Error Pb (%)	Error Pb (ppm)	MPb
1076	43	509400	2.00	10188	0	100.00	0	85600	2.00	1712	206.046
1086	43	481500	2.00	9630	0	100.00	0	81700	2.00	1634	206.046
1154	46	444300	2.00	8886	0	100.00	0	80800	2.00	1616	206.048
1055	42	335749	2.00	6715	1354	4.43	60	55216	2.00	1104	206.047
Mean = 1090 ± 43 Ma [3.9%] 95% conf.; Wtd by data-pt errs only. MSWD = 0.92. probability = 0.43											
945	38	516400	2.00	10328	0	100.00	0	75100	2.00	1502	206.042
969	39	322393	2.00	6448	0	100.00	0	48163	2.00	963	206.042
959	38	515570	2.00	10311	1433	4.19	60	76263	2.00	1525	206.044
1001	40	375641	2.00	7513	0	100.00	0	58213	2.00	1164	206.043
986	39	448147	2.00	8963	220	27.30	60	68319	2.00	1366	206.043
946	38	208956	2.00	4179	1160	5.17	60	30476	2.00	610	206.045
994	40	414200	2.00	8284	0	100.00	0	63700	2.00	1274	206.043
Mean = 971 ± 29 Ma [3.0%] 95% conf.; Wtd by data-pt errs only. MSWD = 0.34. probability = 0.92											
Allanite-(Ce)											
10255	410	0	100.00	0	7770	2.00	155	4603	2.00	92	207.977
10594	424	0	100.00	0	5019	2.00	100	3100	2.00	62	207.977
10314	413	0	100.00	0	5459	2.00	109	3257	2.00	65	207.977
9917	397	0	100.00	0	7111	2.00	142	4037	2.00	81	207.977
10460	418	0	100.00	0	6522	2.00	130	3963	2.00	79	207.977
9926	790	18	100.00	18	1881	3.19	60	3090	2.00	62	207.304
Mean = 10278 ± 350 Ma [3.4%] 95% conf.; Wtd by data-pt errs only. MSWD = 0.36. probability = 0.88											
7909	537	150	40.06	60	5960	2.00	119	5160	2.00	103	207.412
7468	472	211	28.38	60	6891	2.00	138	5252	2.00	105	207.426
7823	516	211	28.38	60	6100	2.00	122	5986	2.00	120	207.336
7761	502	238	25.22	60	6294	2.00	126	6264	2.00	125	207.322
7380	469	326	18.41	60	6135	2.00	123	5986	2.00	120	207.281
7576	598	300	20.03	60	3419	2.00	68	5271	2.00	105	207.131
7482	491	167	35.84	60	6443	2.00	129	4584	2.00	92	207.472
7369	474	62	97.29	60	7392	2.00	148	3582	2.00	72	207.759
7344	478	264	22.70	60	6012	2.00	120	5160	2.00	103	207.340
7429	510	115	52.39	60	5977	2.00	120	3684	2.00	74	207.564
7726	463	308	19.46	60	7551	2.00	151	7702	2.00	154	207.306
7986	579	264	22.70	60	4465	2.00	89	6858	2.00	137	207.178
7916	497	115	52.39	60	7586	2.00	152	5262	2.00	105	207.551
7681	611	652	9.20	60	2127	2.82	60	10134	2.00	203	206.936
7452	657	335	17.92	60	2593	2.31	60	4928	2.00	99	207.059
Mean = 7609 ± 260 Ma [3.4%] 95% conf.; Wtd by data-pt errs only. MSWD = 0.19. probability = 1.000											

Table 2. Cont.

Age (Ma)	Error Age (Ma)	U (ppm)	Error U (%)	Error U (ppm)	Th (ppm)	Error Th (%)	Error Th (ppm)	Pb (ppm)	Error Pb (%)	Error Pb (ppm)	MPb
Allanite-(Ce)											
6471	381	511	11.74	60	6698	2.00	134	4918	2.00	98	207.282
6801	431	62	97.29	60	7718	2.00	154	3183	2.00	64	207.815
6617	396	379	15.84	60	7120	2.00	142	4677	2.00	94	207.380
6446	396	282	21.28	60	7120	2.00	142	3833	2.00	77	207.493
6655	407	1013	5.92	60	2848	2.11	60	7071	2.00	141	206.894
6463	432	308	19.46	60	5344	2.00	107	3396	2.00	68	207.373
6464	418	396	15.13	60	5397	2.00	108	3870	2.00	77	207.295
6411	374	344	17.46	60	7999	2.00	160	4380	2.00	88	207.472
6496	373	467	12.85	60	7691	2.00	154	5085	2.00	102	207.353
6543	369	590	10.16	60	7357	2.00	147	5763	2.00	115	207.259
6544	394	529	11.35	60	6039	2.00	121	4974	2.00	99	207.231
6350	430	678	8.84	60	3147	2.00	63	4250	2.00	85	206.991
6688	514	388	15.48	60	3244	2.00	65	3526	2.00	71	207.127
6578	613	273	21.97	60	2742	2.19	60	2487	2.41	60	207.189
6679	540	493	12.16	60	2540	2.36	60	3907	2.00	78	207.007
Mean = 6535 ± 210 Ma [3.2%] 95% conf.; Wtd by data-pt errs only. MSWD = 0.080. probability = 1.000											
6055	295	1559	3.85	60	5538	2.00	111	7656	2.00	153	206.929
5973	382	106	56.75	60	7806	2.00	156	2784	2.16	60	207.791
5733	306	819	7.32	60	7744	2.00	155	4751	2.00	95	207.243
5801	349	502	11.95	60	6188	2.00	124	3434	2.00	69	207.330
5973	457	220	27.24	60	5002	2.00	100	2329	2.58	60	207.514
5710	330	546	10.98	60	6979	2.00	140	3666	2.00	73	207.351
5987	342	441	13.62	60	7999	2.00	160	4065	2.00	81	207.442
5662	350	220	27.24	60	7709	2.00	154	2868	2.09	60	207.663
5767	345	264	22.70	60	7867	2.00	157	3146	2.00	63	207.612
6034	342	405	14.81	60	8500	2.00	170	4167	2.00	83	207.483
5940	302	0	100.00	0	6364	2.00	127	1949	3.08	60	207.977
5654	323	546	10.98	60	7331	2.00	147	3684	2.00	74	207.373
6029	299	1454	4.13	60	5546	2.00	111	7146	2.00	143	206.947
Mean = 5871 ± 180 Ma [3.1%] 95% conf.; Wtd by data-pt errs only. MSWD = 0.21. probability = 0.998											
5437	303	925	6.49	60	5415	2.00	108	3786	2.00	76	207.093
5197	326	590	10.16	60	5520	2.00	110	2700	2.22	60	207.280
5248	229	2123	2.83	60	8852	2.00	177	6997	2.00	140	206.984
5194	345	300	20.03	60	6847	2.00	137	2431	2.47	60	207.585
5394	317	273	21.97	60	8403	2.00	168	2960	2.03	60	207.651
Mean = 5293 ± 260 Ma [4.9%] 95% conf.; Wtd by data-pt errs only. MSWD = 0.13. probability = 0.97											

Table 2. Cont.

Age (Ma)	Error Age (Ma)	U (ppm)	Error U (%)	Error U (ppm)	Th (ppm)	Error Th (%)	Error Th (ppm)	Pb (ppm)	Error Pb (%)	Error Pb (ppm)	MPb
EPIDOTE											
5850	584	784	7.65	60	0	100.00	0	2571	2.33	60	206.588
5927	553	828	7.25	60	0	100.00	0	2868	2.09	60	206.601
6682	775	626	9.59	60	0	100.00	0	3833	2.00	77	206.720
5642	518	1075	5.58	60	79	75.84	60	3072	2.00	61	206.562
6486	761	617	9.73	60	0	100.00	0	3239	2.00	65	206.692
6115	669	837	7.17	60	149	40.15	60	3369	2.00	67	206.652
5708	311	2238	2.68	60	167	35.93	60	6691	2.00	134	206.574
6160	611	758	7.92	60	0	100.00	0	3109	2.00	62	206.640
5846	542	846	7.09	60	0	100.00	0	2765	2.17	60	206.587
6176	613	758	7.92	60	0	100.00	0	3146	2.00	63	206.643
6006	555	828	7.25	60	0	100.00	0	3035	2.00	61	206.615
6455	766	608	9.87	60	0	100.00	0	3118	2.00	62	206.687
6301	804	687	8.73	60	149	40.15	60	3183	2.00	64	206.683
5866	825	608	9.87	60	26	100.00	26	2023	2.97	60	206.596
6195	690	846	7.09	60	62	97.51	60	3582	2.00	72	206.654
6391	874	529	11.35	60	0	100.00	0	2580	2.33	60	206.677
5882	507	907	6.61	60	0	100.00	0	3044	2.00	61	206.594
6413	919	608	9.87	60	105	56.88	60	3053	2.00	61	206.696
6413	723	828	7.25	60	79	75.84	60	4139	2.00	83	206.689
6637	828	573	10.48	60	0	100.00	0	3387	2.00	68	206.714
6102	799	643	9.33	60	281	21.33	60	2617	2.29	60	206.677
5728	599	899	6.68	60	176	34.13	60	2756	2.18	60	206.593
5982	508	925	6.49	60	0	100.00	0	3332	2.00	67	206.611
6006	895	529	11.35	60	9	100.00	9	1940	3.09	60	206617
6557	958	485	12.38	60	0	100.00	0	2691	2.23	60	206.702
6132	669	828	7.25	60	185	32.50	60	3387	2.00	68	206.659
6174	757	740	8.11	60	97	62.05	60	3100	2.00	62	206.656
5825	495	925	6.49	60	0	100.00	0	2979	2.01	60	206.584
6266	748	731	8.21	60	202	29.68	60	3313	2.00	66	206.684
Mean = 6022 ± 230 Ma [3.8%] 95% conf.; Wtd by data-pt errs only. MSWD = 0.20. probability = 1.000											
URANINITE											
517	21	707293	2.00	14146	0	100.00	0	53666	2.00	1073	206.030
487	19	727010	2.00	14540	0	100.00	0	51810	2.00	1036	206.029
474	19	730173	2.00	14603	0	100.00	0	50641	2.00	1013	206.029
512	21	720218	2.00	14404	686	21.88	150	54158	2.00	1083	206.030
476	19	730138	2.00	14603	0	100.00	0	50827	2.00	1017	206.029

Table 2. Cont.

Age (Ma)	Error Age (Ma)	U (ppm)	Error U (%)	Error U (ppm)	Th (ppm)	Error Th (%)	Error Th (ppm)	Pb (ppm)	Error Pb (%)	Error Pb (ppm)	MPb
URANINITE											
493	20	708853	2.00	14177	861	17.41	150	51253	2.00	1025	206.030
502	20	708544	2.00	14171	993	15.10	150	52191	2.00	1044	206.030
491	20	727997	2.00	14560	0	100.00	0	52348	2.00	1047	206.029
471	19	755149	2.00	15103	396	37.92	150	52061	2.00	1041	206.029
482	19	718350	2.00	14367	2408	6.23	150	50734	2.00	1015	206.031
475	19	730146	2.00	14603	0	100.00	0	50752	2.00	1015	206.029
470	19	717257	2.00	14345	0	100.00	0	49277	2.00	986	206.029
502	20	709892	2.00	14198	334	44.91	150	52302	2.00	1046	206.030
494	20	729618	2.00	14592	0	100.00	0	52812	2.00	1056	206.029
478	19	748947	2.00	14979	0	100.00	0	52404	2.00	1048	206.029
517	21	745300	2.00	14906	0	100.00	0	56600	2.00	1132	206.030
473	19	713205	2.00	14264	7076	2.12	150	49435	2.00	989	206.035
479	19	719812	2.00	14396	7454	2.01	150	50567	2.00	1011	206.035
502	20	703020	2.00	14060	0	100.00	0	51764	2.00	1035	206.030
500	20	714817	2.00	14296	0	100.00	0	52386	2.00	1048	206.030
478	19	714271	2.00	14285	0	100.00	0	49964	2.00	999	206.029
474	19	712333	2.00	14247	0	100.00	0	49351	2.00	987	206.029
519	21	710588	2.00	14212	0	100.00	0	54158	2.00	1083	206.030
474	19	738023	2.00	14760	0	100.00	0	51142	2.00	1023	206.029
503	20	703382	2.00	14068	11146	2.00	223	52172	2.00	1043	206.039
504	20	715346	2.00	14307	0	100.00	0	52896	2.00	1058	206.030
482	19	709927	2.00	14199	0	100.00	0	50047	2.00	1001	206.029
500	20	696730	2.00	13935	0	100.00	0	51124	2.00	1022	206.030
477	19	696607	2.00	13932	0	100.00	0	48590	2.00	972	206.029
501	20	736023	2.00	14720	0	100.00	0	54084	2.00	1082	206.030
Mean = 489.3 ± 7.0 Ma [1.4%] 95% conf.; Wtd by data-pt errs only. MSWD = 0.60. probability = 0.95											
ORDINARY URANOPHANE											
26	1	499500	2.00	9990	7600	2.00	152	1800	3.33	60	206.029
26	1	445100	2.00	8902	0	100.00	0	1600	3.75	60	206.020
28	1	480900	2.00	9618	0	100.00	0	1900	3.16	60	206.020
26	1	500900	2.00	10018	10600	2.00	212	1800	3.33	60	206.033
29	2	436500	2.00	8730	30500	2.00	610	1800	3.33	60	206.062
26	4	333027	2.00	6661	932	16.10	150	1234	12.15	150	206.022
27	3	527948	2.00	10559	3279	4.58	150	1995	7.52	150	206.024
Mean = 26.7 ± 1.2 Ma [4.5%] 95% conf.; Wtd by data-pt errs only. MSWD = 0.81. probability = 0.56											

Table 2. Cont.

Age (Ma)	Error Age (Ma)	U (ppm)	Error U (%)	Error U (ppm)	Th (ppm)	Error Th (%)	Error Th (ppm)	Pb (ppm)	Error Pb (%)	Error Pb (ppm)	MPb
AUTUNITE											
13	2	551321	2.00	11026	0	100.00	0	1002	14.97	150	206.020
9	2	552924	2.00	11058	0	100.00	0	687	21.84	150	206.019
12	2	538846	2.00	10777	0	100.00	0	919	16.33	150	206.020
10	2	522565	2.00	10451	0	100.00	0	733	20.46	150	206.020
9	3	425382	2.00	8508	0	100.00	0	538	27.87	150	206.019
11	2	524080	2.00	10482	0	100.00	0	817	18.37	150	206.020
13	2	551321	2.00	11026	0	100.00	0	984	15.25	150	206.020
10	3	457512	2.00	9150	0	100.00	0	631	23.77	150	206.019
9	2	545013	2.00	10900	0	100.00	0	696	21.55	150	206.019
10	2	519244	2.00	10385	0	100.00	0	715	20.99	150	206.019
12	2	547075	2.00	10941	0	100.00	0	882	17.01	150	206.020
13	2	519200	2.00	10384	0	100.00	0	928	16.16	150	206.020
Mean = 10.9 ± 1.3 Ma [12%] 95% conf.; Wtd by data-pt errs only. MSWD = 0.48. probability = 0.92											

It is probable that older uraninite crystals of albitites experienced recent lead loss, since the 500 Ma metamorphic event can not be seen in figure 8A. However, due to robust crystal structure, lead loss did not take place in albitite zircon after the 500 Ma metamorphic event. General and specific geological information can be withdrawn from the mineral ages presented in table 2 and figures 7 and 8.

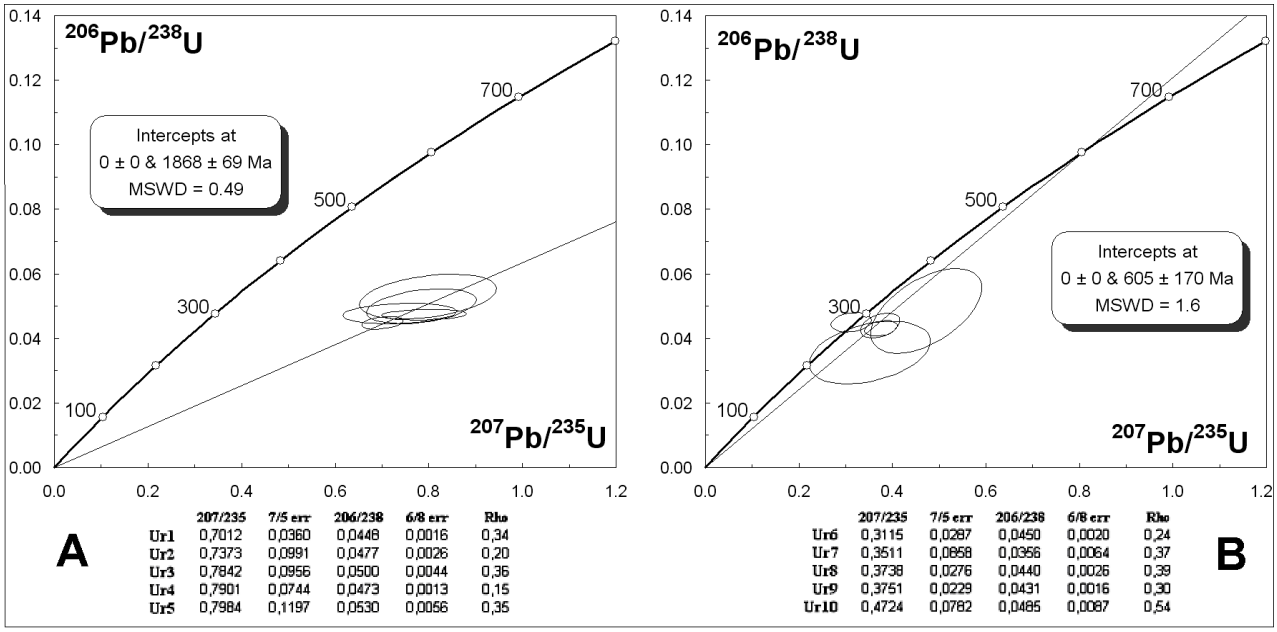

Figure 8. Pb discordias anchored to 0 Ma for two uraninite groups of albitites (metamorphosed syenites). Diagram 8A represents older uraninite group (garnet related) and diagram 8B represents younger one (epidote related). Error ellipses are 2s for the older ones and 1s for the younger ones. Data sheet is also shown.

4.3. Zircon

Very low concentrations of U and Pb, close to detection limits of electron microprobe led to large age errors, which made zircon unable to be dated by this technique. Thus, zircon age of 847 ± 680 Ma has no geological significance. In fact, Cocherie & Legendre (2007) show that electron microprobe is not a reliable method for dating zircon. LA-ICP-MS technique, however, seems to be good for dating this mineral. The age of 1904 ± 44 Ma, corresponding to the upper intercept, and the age of 483 ± 100 Ma, corresponding to the lower intercept, can be respectively interpreted as Orosirian and Brasiliano metamorphic events recorded by zircon. Therefore, zircon is good to date metamorphism but it is not useful to date hydrothermal events. It is important to point out that Orosirian age can also represent magmatic crystallization of zircon, which occurred inside shear zones, an environment of robust deformation.

4.4. Uraniferous titanite and Fe and (radiogenic) Pb-rich "uranophane"

The highest age found for uraniferous titanite by electron microprobe was 2052 ± 80 Ma (Table 2). Since several regional syenites and peraluminous sodic granites have been dated between 2100 Ma and 2000 Ma (CPRM-CBPM, 2003; Guimarães *et al*., 2005), the age 2052 ± 80 Ma possibly means magmatic crystallization of the albitite parent rock (probable syenite).

In opposition to zircon, uraniferous titanite and Fe and (radiogenic) Pb-rich "uranophane" have proved to be good minerals for recording hydrothermal processes. Tetravalent uranium released from uraniferous titanite, initially precipitating as uraninite (Figs. 3 and 9), was oxidized to yield hexavalent uranium anionic complexes during successive Proterozoic hydrothermal events. Along with Ca and Fe cations from augite of the rock, these complexes precipitated mainly as channels of Fe and (radiogenic) Pb-rich "uranophane". Successive concordant ages for both uraniferous titanite and Fe and (radiogenic) Pb-rich "uranophane" point out to five hydrothermal events: 1701 ± 57 Ma and 1715 ± 60 Ma are the record of the first one, 1488 ± 64 Ma and 1491 ± 52 Ma are the record of the second one, 1298 ± 69 Ma and 1309 ± 36 Ma are the record of the third one, 1108 ± 78 Ma and 1090 ± 43 Ma are the record of the fourth one, and finally 978 ± 50 Ma and 971 ± 29 Ma are the record of the fifth one. Remarkably, Brasiliano metamorphic event was not recorded by both minerals.

The ca. 1.7 Ga hydrothermal event is probably related to fluids yielded during ca. 1.7 Ga anorogenic São Timóteo Granite emplacement. The ca. 1.5 Ga hydrothermal event is probably related to lithospheric mantle activation process that led to extensional episodes in Lagoa Real region. This process is recorded by 1.5 Ga basic rocks (U-Pb by Babinski *et al*., 1999; Guimarães *et al*., 2005) and 1.5 Ga muscovite-martite dykes and sills (Ar-Ar by Battilani *et al*., 2007) crosscutting regional rocks. The ca. 1.3 Ga event could be the record of hydrothermal fluids related to extensional event marked by 1.25 Ga Januária mafic dykes (Chaves & Neves, 2005), which are regionally found. The ca. 1.1 Ga and ca. 0.97 Ga events are probably linked to hydrothermalism yielded during Rodinia supercontinent breakup (D'Agrella-Filho *et al*., 1990; Weil *et al*., 1998), which certainly attained the Lagoa Real region. Chaves & Neves (2005) also show 1.0-0.9 Ga Formiga mafic dyke swarm close to the study region, which is related to extensional event during Rodinia breakup.

Light and dark portions can be observed in titanite WDS backscattered electron image (Fig. 9A) and probably represent the record of these five hydrothermal events. Corfu & Stone (1998), Frost *et al*. (2000), and Jung & Hellebrand (2007) have also found similar features in uranium-bearing titanite crystals, which demonstrate that titanite can contain multiple age domains, preserving a chronological and chemical record of successive hydrothermal events.

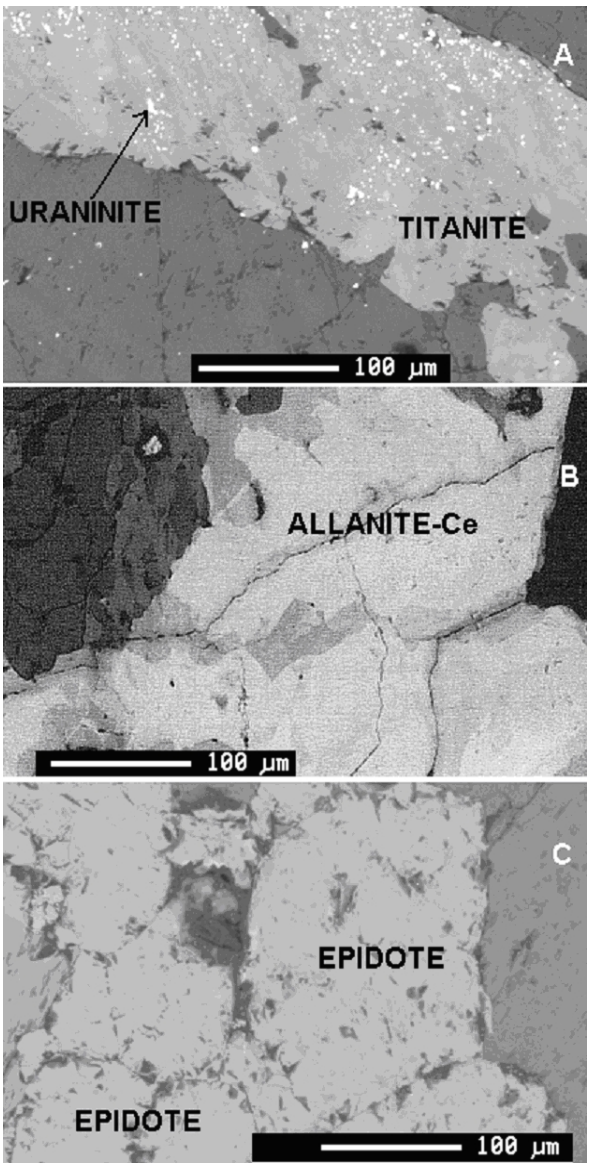

Figure 9. WDS backscattered electron images showing titanite (A), allanite-(Ce) (B), and epidote (C).

4.5. Allanite-(Ce)

Likewise titanite, allanite-(Ce) shows heterogeneity which is revealed by WDS backscattered electron image (Fig. 9B). The analyses of light and dark portions, however, seem to point out to successive radiogenic lead incorporation by allanite-(Ce) during the five hydrothermal events found by titanite and Fe and (radiogenic) Pb-rich "uranophane" dating. Such successive incorporations yielded five very old ages by electron microprobe: 5293 ± 260 Ma, 5871 ± 180 Ma, 6535 ± 210 Ma, 7609 ± 260 Ma, and 10278 ± 350 Ma. Therefore, allanite-(Ce) can not be used to find precise ages of multiple hydrothermal events, although it can indirectly reveal them. Lead mobilization can also be attested by galena rarely found in some albitite bodies. Such galena probably crystallized with radiogenic lead mainly from titanite.

4.6. Uraninite

By using LA-ICP-MS technique, two different uraninite groups were identified in terms of their isotopic ratios, one andradite-related uraninite and another for epidote-related uraninite. The first uraninite group shows a U-Pb system starting from a 1868 ± 69 Ma metamorphic episode (Fig. 8A). Despite the large error, the age of 605 ± 170 Ma (Fig. 8B) for uraninite crystals of the second group reveals another metamorphic event. This younger metamorphic event (Brasiliano) was best constrained by electron microprobe uraninite age of 489.3 ± 7.0 Ma. Majority of uraninite that was analyzed by electron microprobe are the ones found inside epidote crystals. Ar-Ar ages between 485 Ma and 500 Ma have been found for micas of shear zones which promoted transformations in albitites during Brasiliano structural reactivation (Silva *et al*., 2006) and seem to make the uraninite age of 489.3 ± 7.0 Ma reliable.

4.7. Epidote

Electron microprobe epidote age of 6022 ± 230 Ma reveals that it can not be used to date any geological event. In order to explain the age of ca. 6000 Ma, the epidote would appear during Brasiliano metamorphic event (uraninite found inside epidote has ca. 490 Ma), when it would have incorporated lead. Pb incorporation probably took place only during this event since the heterogeneity seen in allanite-(Ce) and titanite is not shown by WDS backscattered electron image of epidote (Fig. 9C).

4.8. Ordinary uranophane and autunite

Percolation of meteoric waters in albitites during Cenozoic led to precipitation of calcite and ordinary uranophane at 26.7 ± 1.2 Ma in rock microfractures. Probable interaction between soluble uranyl complexes and apatite crystals of the albitites finally led to precipitation of autunite at 10.9 ± 1.3 Ma. Only ordinary uranophane and autunite have not been crystallized from thermal or metamorphic events among dated minerals.

Under the light of global tectonics, Plant *et al*. (1999) point out that many uraniferous provinces are related to felsic igneous rocks intruded in the crust, not only anorogenically but also during the final stages of orogenesis. According to Bonin (1987), during the late orogenic stages, ductile shear zones control the site of emplacement of felsic magmatic provinces. Pressure release caused by the faulting can produce partial melting in deep zones in the thickened orogenic lithosphere. Furthermore, magmas derived from the partial melting of the lithospheric mantle above the subducted slab are sponsored by the dehydration of the latter. The interaction between fluids generated during this dehydration and overlying mantle material would be responsible for the trace and rare earth elements, thorium, and uranium enrichment in magmas (Keppler, 1996). When submitted to fractional crystallization processes such magmas eventually generate uraniferous felsic magmatic provinces.

According to regional geology, albitite bodies outcrop in association to amphibolite lenses along shear zones and both lithologies are hosted by microcline gneisses (cross section in Fig. 1). It is reliable to suppose that a basic magma (current amphibolite) differentiated to intermediate magma (current albitite), which in its turn evolved to acid magma (current microcline gneiss) during final stages of the Orosirian Orogeny. LA-ICP-MS U-Pb zircon age of 2009 ± 78 Ma (Fig. 10) interpreted as magmatic crystallization (similar to electron microprobe titanite age of 2052 ± 80 Ma), has also been found for microcline gneisses and supports this hypothesis. Such scenario is different from the previous metasomatic models (e.g. Maruéjol, 1989; Lobato & Fyfe,1990; Cruz, 2004) which propose albitization and total quartz removal of the ca. 1.7 Ga São Timóteo Granite. Therefore, we suggest the idea of sodic syenite as protolith of the albitites. It is important to rephrase that several regional syenites and granites have been dated around 2000 Ma (CPRM-CBPM, 2003; Guimarães *et al*., 2005).

Based on isotopic U-Pb titanite age, Pimentel *et al.* (1994) concluded that uranium mineralization found in albitites would have ca. 1.0 Ga. Supported by isotopic U-Pb age on heavy minerals and uraninite separate from albitites, Turpin *et al*. (1988) concluded that mineralization would have ca. 1.3 Ga. In both researches, these authors suggest remobilization of the uranium mineralization at ca. 500 Ma. According to our geochronological data, 0.96 Ga and 1.3 Ga represent two of the multiple hydrothermal events imposed on ca. 2000 Ma albitites (sodic syenites). The remobilization of 500 Ma is in agreement with our data.

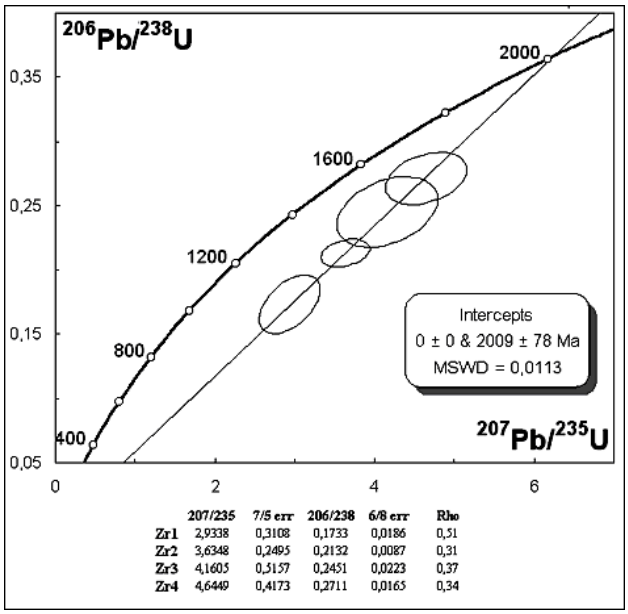

Figure 10. Zircon U-Pb discordia (anchored to 0 Ma) of microcline-gneisses. Error ellipses are 2s. Data sheet is also shown.

5.Conclusions

In addition to new petrographical data, geochronological scenario presented here questions previous metasomatic models for Lagoa Real albitites and uranium mieralization. Electron microprobe chemical U-Th-Pb and LA-ICP-MS U-Pb dating of minerals of albitites suggest protolith (uraniferous sodic syenites) crystallization and isochemical metamorphism at ca. 2.0-1.9 Ga during the late stages of the Orosirian orogenic event, when a first generation of uraninites was formed. Multiple uranium and lead mobilization promoted by at least five hydrothermal events (ca. 1.7 Ga, ca. 1.5 Ga, ca. 1.3 Ga, ca. 1.1 Ga and ca. 1.0 Ga) was detected in such rocks. A probable generation of a second uraninite group and/or resetting of U-Pb clock of older uraninites during the Brasiliano orogenic event at *ca*. 0.5 Ga also took place.

Acknowledgments - We would like to address special thanks to CNPq for the first author's Post Doctoral research support (Grant 154987/2006-9), to the Center for Development of Nuclear Technology (CDTN-CNEN) and Physics Department of Minas Gerais Federal University (UFMG) where the work was developed with unrestricted support, to Memorial University of Newfoundland (Canada) where geochronological studies by LA-ICP-MS were carried out, and to Brazilian Nuclear Industries (INB) for field work and sampling support. We are also grateful to Alain Cocherie on providing EPMA software and to Luiz A. Garcia and Ivan M. Araújo by helping on electron microprobe analyses.

References

Almeida F.F. 1977. O Cráton do São Francisco. *Revista Brasileira de Geociências,* 7: 349-364.

Alves J.V. & Fuzikawa K. 1984. O estudo de inclusões fluidas da jazida uranífera de Cachoeira-Caetité, BA: resultados preliminares. In: CONGRESSO BRASILEIRO DE GEOLOGIA, 33., 1984, Rio de Janeiro. *Anais... SBG*, v.3. p.1503-1517.

Babinski M., Pedreira A., Neves B. B. B., Van Schmus W. R. 1999. Contribuição à geocronologia da Chapada Diamantina. In: SIMPÓSIO NACIONAL DE ESTUDOS TECTÔNICOS, 7.,1999, Lençóis, *Anais...,* Bahia, p. 118-120.

Battilani G. A., Gomes N. S., Guerra W. J. 2007. The occurrence of microdiamonds in Mesoproterozoic Chapada Diamantina intrusive rocks - Bahia / Brazil. *Anais da Academia Brasileira de Ciências*, 79 (2): 321-332.

Bonin B. 1987. From orogenic to anorogenic magmatism: a petrological model for the transition calc-alkaline - alkaline complexes. *Revista Brasileira de Geociências*, 17(4): 366-371.

Caby R. & Arthaud M. 1987. Petrostructural evolution of the Lagoa Real subalkaline metaplutonic complex (Bahia, Brazil). *Revista Brasileira de Geociências*, 17:636.

Chaves A. O. & Neves, J. M. C. 2005. Radiometric ages, aeromagnetic expression and general geology of mafic dykes from southeastern Brazil and implications for African-South American correlations. *Journal of South American Earth Sciences*, 19 (3): 385-394.

Chaves, A. O. ; Tubrett, M. ; Rios F J . ; Oliveira, L. A. R. ; Alves, J. V. ; Fuzikawa, K. ; Neves, J. M. C. ; Mattos, E. C. ; Chaves, A. M. D. V.; Prates, S. P. 2007. U-Pb ages related to uranium mineralization of Lagoa Real, Bahia - Brazil: tectonic implications. *Revista de Geologia*, 20 (2):141-156.

Cocherie A. & Legendre O. 2007. Potential minerals for determining U-Th-Pb chemical age using electron microprobe. *Lithos* 93: 288–309.

Cordani U.G. & Brito Neves. 1982. The geologic evolution of South America during the Archaean and Early Proterozoic. *Revista Brasileira de Geociências*, 12:78-88.

Cordani U.G., Iyer S.S., Taylor K., Kawashita K., Sato K., McReath I. 1992. Pb-Pb, Rb-Sr, and K-Ar systematics of the Lagoa Real uranium province (south-central Bahia, Brazil) and the Espinhaço Cycle (ca. 1.5-1.0 Ga). *Journal South American Earth Science*, 5:33-46.

Corfu F. & Stone D. 1998. The significance of titanite and apatite U-Pb ages: Constraints for the post-magmatic thermal-hydrothermal evolution of a batholithic complex, Berens River area, northwestern Superior Province, Canada. *Geochimica et Cosmochimica Acta*, 62(17): 2979–2995.

Costa P.H.O., Andrade A.R..F, Lopes G.A., Souza S.L. 1985. *Projeto Lagoa Real: Mapeamento Geológico*, *1:25.000*. 98p. Salvador, CBPM, v.1.

CPRM. Companhia de Pesquisas de Recursos Minerais. 1995. *Catálogo geral de produtos e serviços*. *Geologia. Levantamentos Aerogeofísicos. Base de dados Aerogeofísicos.* Rio de Janeiro, Geologia e Recursos Hídricos, 367 p.

CPRM/CBPM. 2003. *Geologia e Recursos Minerais do Estado da Bahia – Sistema de Informações Geográficas*. CD-ROM.

Cruz S. C. P. 2004. *A interação entre o Aulacógeno do Paramirim e o Orógeno Araçuaí-Oeste Congo*. Ouro Preto, 505p. Tese Doutorado, Contribuições as Ciências da Terra - Série D, Universidade Federal de Ouro Preto.

D'Agrella-Filho M. S., Pacca I. G., Renne P. R., Onstott T. C., Teixeira W. 1990. Paleomagnetism of Middle Proterozoic (1.01 to 1.08 Ga) mafic dykes in southeastern Bahia State - São Francisco Craton, Brazil. *Earth Planetary Science Letter*, 101: 332-348.

Finch R. & Murakami T. 1999. Systematics and Paragenesis of uranium minerals. In: Uranium: Mineralogy, Geochemistry and the Environment. In: Burns & Finch (Eds). *Reviews in Mineralogy*. V. 38. p. 91-166.

Frost B. R., Chamberlain K.R., Schumacher J. C. 2000. Sphene (titanite): phase relations and role as a geochronometer. *Chemical Geology*, 172:131–148.

Garrido I.A.A., Silva R.W.S, Mascarenhas J.F. 2002. *Interpretação integrada de dados magnéticos e gamaespectrométricos - Área Ibitiara-Rio das Contas, Bahia, Brasil*. Programa de Levantamentos Aerogeofísicos - CBPM. 15p.

Geisel Sobrinho, E. 1981. *Apresentação de uma hipótese genética para o Distrito Uranífero de Lagoa Real*. Nota Técnica EBHO.PM N° 3., NUCLEBRAS, 35p.

Gregory M.J., Wilde A.R., Jones P. 2005. Uranium deposits of the Mount Isa region and their relationship to deformation, metamorphism and Cu deposition. *Economic Geology*, 100:537-546.

Guimarães J.T., Teixeira L.R., Silva M.G., Martins A.A.M, Andrade Filho E.L., Loureiro H.S.C., Arcanjo J.B., Dalton de Souza J., Neves J.P., Mascarenhas J.F., Melo

R.C., Bento R.V. 2005. Datações U-Pb em rochas magmáticas intrusivas no Complexo Paramirim e no Rifte Espinhaço: uma contribuição ao estudo da evolução geocronológica da Chapada Diamantina. In: SIMPOSIO DO CRATON SÃO FRANCISCO, 3, 2005, Salvador. *Anais...,* Bahia, CD-ROM, ST4/07.

Inda H.V.A. & Barbosa J.S.F. 1996. Texto explicativo para o mapa geológico do Estado da Bahia (1:1.000.000). *In:* J.S.L. Barbosa & J.M.S. Dominguez (Eds.). *Geologia da Bahia (texto explicativo).* Salvador, Secretaria da Industria, Comércio e Mineração, Superintendência de Geologia e Recursos Minerais, 400 p.

Jung S. & Hellebrand E. 2007. Textural, geochronological and chemical constraints from polygenetic titanite and monogenetic apatite from a mid-crustal shear zone: An integrated EPMA, SIMS, and TIMS study. *Chemical Geology*, 241: 880-107.

Keppler H. 1996. Constraints from partitioning experiments on the composition of subduction-zone fluids. *Nature*, 380: 237-240.

Kojima S., Takeda S., Kogita S. 1994. Chemical factors controlling the solubility of uraninite and their significance in the genesis of unconformity-related uranium deposits. *Mineralium Deposita*, 29 (4): 353-360.

Langmuir D. 1997. Aqueous Environmental Geochemistry, Prentice-Hall, N. Jersey, USA. 456p.

Lobato L.M. & Fyfe W.S. 1990. Metamorphism, Metasomatism, and Mineralization at Lagoa Real, Bahia, Brazil. *Economic Geology*, 85: 968-989.

Ludwig, K. R. 2003. *Isoplot/Ex 3.00: a geochronological toolkit for Microsoft Excel*. Berkeley Geochronology Center. Special Publication N° 4, 70 p.

Maruéjol P. 1989. *Métasomatose alcaline et minéralisations uranifères: les albitites du gisement de Lagoa Real (Bahia, Brésil) et exemples complémentaires de Xihuashan (SE Chine), Zheltorechensk (Ukraine) et Chhuling Khola (Népal central).* Nancy, 287p. These Docteur, Centre de Recherches sur la Géologie de l'Uranium, France.

Mascarenhas J.F. 1973. A geologia do centro-leste do Estado da Bahia. In: CONGRESSO BRASILEIRO DE GEOLOGIA, 27., 1973, Aracaju. *Anais...,* Aracaju, SBG, v. 2, p. 35-66.

Oliveira A.G., Fuzikawa K., Moura L.A.M., Raposo C. 1985. Província uranífera de Lagoa Real – BA. *In: Principais Depósitos Minerais do Brasil – DNPM*. Vol. I, p.105-120.

Pascholati E.M., Silva C.L., Costa S.S., Osako L.S., Amaral G., Rodriguez I.P. 2003. Novas ocorrências de urânio na região de Lagoa Real, a partir da superposição de dados geofísicos, geológicos e de sensoriamento remoto. *Revista Brasileira de Geociências*, 33 (2-suplemento): 91-98.

Pickhardt C., Dietze H.J., Becker J.S. 2005. Laser Ablation Inductively Coupled Plasma Mass Spectrometry for direct isotope ratio measurements on solid samples. Internat. J. Mass Spectrometry, 242:273-280.

Pimentel M.M., Machado N., Lobato L.M. 1994. Geocronologia U-Pb de rochas graníticas e gnáissicas da região de Lagoa Real (BA) e implicações para a idade da mineralização de Urânio. In: CONGRESSO BRASILEIRO DE GEOLOGIA, 38., 1984, Camboriú . *Anais...,* Florianópolis, SBG, p. 389-390.

Plant J.A., Simpson P.R., Smith B., Windley B. 1999. Uranium ore deposits – products of the radioactive Earth. In: Burns, P.C. & Finch, R. (Eds.) - Uranium: Mineralogy, Geochemistry and the Environment. *Reviews in Mineralogy*, 33: 255-307.

Pommier A., Cocherie A., Legendre O. 2004. *EPMA Dating: age calculation from electron probe microanalyzer measurements of U-Th-Pb*. BRGM, Orléans, France, 9p.

Ribeiro C. I., Carvalho Filho C. A., Hashizume S. 1984. As jazidas de urânio de Lagoa Real. In: CONGRESSO BRASILEIRO DE GEOLOGIA, 38., 1984, Camboriú . *Anais...,* Florianópolis, SBG, p. 1463-1474.

Silva M.G., Guimarães J., Teixeira L., Martins A., Edgard Filho, Loureiro H., Arcanjo J., Souza J., Neves J.P., Mascarenhas J., Melo R., Bento R.V. 2006. Evidências estruturais, metalogenéticas e geocronológicas da inversão neoproterozóica do Rifte do Espinhaço. In: CONGRESSO BRASILEIRO GEOLOGIA, 43., 2006, Aracaju. *Abstracts…*, Aracaju, SBG p.177.

Sylvester P. 2001. *Laser Ablation-ICP-MS- Principles and Applications*. Short Courses Series, v.29. Mineralogical Association of Canada, 243 p.

Turpin L., Maruejol P., Cuney M. 1988. U-Pb, Rb-Sr and Sm-Nd chronology of granitic basement, hydrotermal albitites and uranium mineralization (Lagoa Real, South-Bahia, Brazil). *Contributions to Mineralogy and Petrology*, 98: 139-147.

Weil A.B, Van der Voo R., Niocaill C.M., Meert J.G. 1998. The Proterozoic supercontinent Rodinia: paleomagnetically derived reconstructions for 1100 to 800 Ma. *Earth Planetary Science Letter*, 154: 13–24.

Yardley B.W.D. 1989. *Introdução à Petrologia Metamórfica*. EDUNB (trad.). Brasília. 340p.